Spin–Spin Interaction of TEMPO Molecular Chains Formed in an Organic One-Dimensional Nanochannel as Studied by Electron Spin Resonance (ESR)

Hirokazu Kobayashi,[1] Takahiro Ueda,*[1,2] Keisuke Miyakubo,[2] Taro Eguchi,[1,2] and Atsushi Tani[3]

[1]The Museum of Osaka University, Osaka University, Toyonaka, Osaka 560-0043

[2]Department of Chemistry, Graduate School of Science, Osaka University, Toyonaka, Osaka 560-0043

[3]Department of Earth and Space Science, Graduate School of Science, Osaka University, Toyonaka, Osaka 560-0043

Received September 7, 2006; E-mail: ueda@museum.osaka-u.ac.jp

The magnitude and dimensionality of spin–spin interactions among 2,2,6,6-tetramethyl-1-piperidinyloxyl radical (TEMPO) molecules in a 1D nanochannel consisting of tris(*o*-phenylenedioxy)cyclotriphosphazene (TPP) were examined using electron spin resonance (ESR) spectroscopy. Dilution of TEMPO with 2,2,6,6-tetramethyl-1-piperidine (TEMP), a diamagnetic molecule, reduced the dipolar interaction in the TPP/(TEMPO/TEMP) inclusion compound (IC), leading to axially symmetric hyperfine coupling and *g*-tensors with a molar fraction of 0–0.45: $A_{\perp} = 1.93 \pm 0.03$ mT and $A_{\parallel} = 0.7 \pm 0.1$ mT, and $g_{\perp} = 2.0063 \pm 0.0003$ and $g_{\parallel} = 2.0068 \pm 0.0005$. The resonance line in TPP/(TEMPO/TEMP) IC narrowed when the molar fraction was more than 0.7, implying the existence of exchange narrowing. The ESR lineshape of TPP/TEMPO IC showed pure 1D spin diffusion between 139 and 166 K, while interchain exchange interactions contributed to the line shape in $T > 166$ K. The magnitude of intra-chain exchange interaction, $|J_{\mathrm{intra}}|/k_{\mathrm{B}}$, in TPP/TEMPO IC depended on the temperature from ≈0.05 K in 139–166 K to 0.4 K at 383 K. This aspect implies that molecular motion strongly affects the spin–spin interaction between TEMPO molecules in the TPP crystal. The magnetic susceptibility of TPP/TEMPO IC was also measured, and it was found that the exchange interaction was antiferromagnetic.

The remarkable physical and chemical properties of materials with one-dimensional (1D) atomic or molecular arrangement in the nanochannel are important for developing future devices based on molecular sized functional units.[1–3] Regarding magnetic properties of such materials, a 1D molecular arrangement in the nanochannel is needed to achieve spin crossover[4] or magnetic transition to the 1D antiferromagnetic chain.[5] Such molecular magnetic materials are expected to be promising candidates for future applications in the areas of high-density information storage and quantum computing.[6] Recently, materials with 1D ferro/ferrimagnetic spin arrangement that show spontaneous magnetization below 20 K have been synthesized using metal complexes.[7–12] From a statistical mechanical point of view, the 1D spin chain is known to achieve long range order only at absolute zero. However, if the ratio of the intrachain to the interchain exchange interaction increases and if the spins that constitute the 1D ferro/ferrimagnetic Ising-type chain exhibit strong uni-axial anisotropy, then the relaxation time of the magnetization becomes long (Glauber's theory[13–15]).

As a novel concept for production of materials with 1D spin arrangement, we have reported the inclusion compound (IC) involving the 2,2,6,6-tetramethyl-1-piperidinyloxyl (TEMPO) radical in a porous material with a 1D nanochannel, namely, tris(*o*-phenylenedioxy)cyclotriphosphazene (TPP; see Fig. 1) (TPP/TEMPO IC).[16] This material with a 1D spin arrangement is prepared using only organic materials. Therefore, it

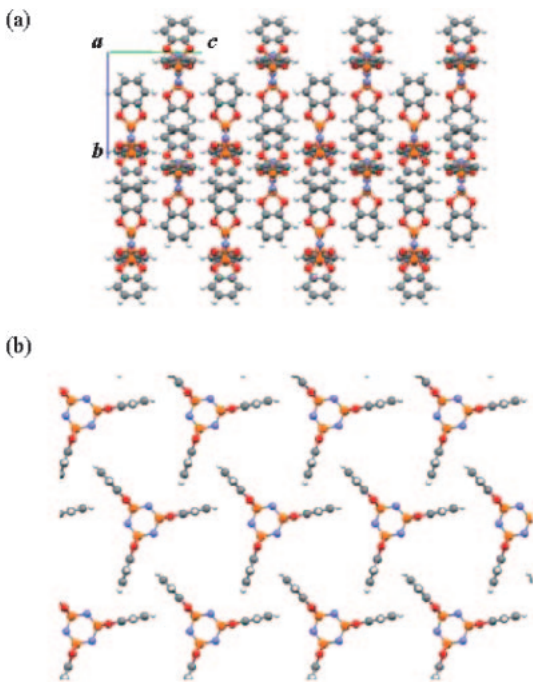

Fig. 1. Guest-free TPP crystal structure along crystal and *a* (a) or *c* axis direction (b).

Published on the web April 13, 2007; doi:10.1246/bcsj.80.711

is suggested that the unpaired electron consisting of 1D spin arrangement is localized on the p_z orbital on the nitroxide group of TEMPO molecule. A typical organic zeolite, TPP has a homogeneous nanochannel structure with a minimum diameter of 0.46 nm in guest-free states.[17] It forms inclusion compounds through recrystallization from benzene or other organic solvents.[17–24] A stable nanochannel is achieved through desorption of the guest molecules by heating.[21] Using TPP as a template, various functional ICs have been developed by Hulliger and co-workers, e.g., TPP/I_2 IC with electric conductivity along the nanochannel ($\sigma_{\parallel} \approx 10^{-6}$–$10^{-8}\ \Omega^{-1}\,m^{-1}$, in a potential of 50 V),[25] and ICs with nonlinear optical molecules.[26] Furthermore, they have attempted to prepare TPP/TTTA IC (TTTA = 1,3,5-trithia-2,4,6-triaza-2*H*-pentalen-2-yl radical) with a 1D spin chain.[27] However, since TTTA, a heterocyclic organic radical,[28–30] is unstable in ambient conditions and since it is difficult to prepare a good quality IC and homogeneous 1D spin chain,[27] the handling of TTTA and detailed examination of its spin–spin interaction of TPP/TTTA IC is not straightforward.

On the other hand, we have used TEMPO,[31–33] a representative nitroxide radical molecule,[34] as a spin source in the production of materials with 1D spin arrangement[16] because it is stable and because it should be possible to prepare various ICs with organic radical molecules. We have shown, using thermogravimetry (TG), powder X-ray diffraction (XRD), and chemical analysis, that TPP/TEMPO IC accommodates one TEMPO molecule in the TPP unit cell.[16] The ESR spectrum of TPP/TEMPO IC depends on the preparation method, and in the recrystallization method, an isotropic resonance line with peak-to-peak linewidth of 1.8 mT is observed, whereas in the adsorption method, the ESR spectrum is given by the superposition of an isotropic broad line and a triplet split by hyperfine coupling with ^{14}N nuclei. The spectra of TPP/TEMPO IC are sensitive to the difference in the spin–spin interaction of the 1D spin chain. This spin–spin interaction can be related to the interspin distance in 1D spin chain constructed in the TPP nanochannel; the interaction affects the magnetic properties of TPP/TEMPO IC. However, experimental evidence and discussion of the relationship with the interspin distance for dimensionality and quantitative evaluation of the magnitude of spin–spin interaction have not yet been given in this system.

In this study, we specifically examined the dependence of the spin–spin interaction of TPP/TEMPO IC on the interspin distance in the TPP nanochannel. The dilution of spins with diamagnetic 2,2,6,6-tetramethyl-1-piperidine (TEMP) molecules enabled us to identify the origin of the spin–spin interaction leading to line broadening and to elucidate the exchange narrowing of the ESR spectrum and dimensionality of the exchange interaction. In addition, the sign of the exchange interaction was examined by magnetic susceptibilities measurements.

Experimental

Sample Preparation. TPP was synthesized using processes described in the literature.[16] For purification, the synthesized specimen was recrystallized twice from a benzene solution. A guest free TPP powder specimen was prepared by heating at 348 K for 3 h under reduced pressure.[35] From Wako Pure Chemical Industries Ltd., TEMPO radical and 2,2,6,6-tetramethyl-1-piperidine (TEMP) were purchased; they were used without further purification. From a mesitylene solution containing TPP and TEMPO and/or TEMP, TPP/TEMPO IC was recrystallized at an appropriate ratio. For example, when a molar fraction of TEMPO (x_{TEMPO}) is 0.017, TPP was recrystallized in 1 mL mesitylene with 1 mL TEMPO/TEMP = 1/100 solution. The content of guest molecules and ratio of TEMPO in the guest molecules were determined by thermogravimetry (TG), chemical analysis, and ESR spin concentration (see below). All crystallites were filtered and dried in air without washing to avoid the solvation of the inclusion compound. All crystallites were needle-shaped, and the color was dependent on the ratio of TEMPO to all guest compounds, e.g., light orange in TPP/TEMPO IC, and colorless in TPP/TEMP IC. The formation of the IC was confirmed by powder XRD.

ESR Measurements. Powder ESR spectra were recorded on an X-band spectrometer (RE-1X; JEOL). In TPP/TEMPO IC, temperature dependence of the ESR spectra was carried out in the range of 12–383 K. Powdered specimens of 0.35–6.82 mg were packed in an ESR tube (270 mm length and o.d. 5 mmϕ) made from quartz glass, and then, the tubes were capped with plastic cap. In 108–383 K, ESR measurements were carried out under dried air atmosphere. In general, ESR signal from O_2 gas was observed only in the low-pressure region from 10^{-3} to 10^{-1} MPa where strong spin–spin interactions becomes weak.[36] Therefore, the influence by O_2 gas on the ESR measurements was negligible under dried air atmosphere because of the strong spin–spin interaction between O_2 molecules and the intense signal from TPP/TEMPO IC and/or TPP/(TEMPO/TEMP) IC. We also confirmed that guest-free TPP polycrystalline sample did not give an ESR signal under dried air atmosphere. ESR measurements for TPP/TEMPO IC below 108 K were carried out under reduced pressure, 10^{-3} MPa. In this temperature range, no signal was observed from the empty ESR tube under reduced pressure. Thermal equilibrium of the sample was achieved by waiting 10–20 min after temperature changes. We also confirmed the signal reproduction by cycling the temperature. The power of the X-band microwave was set to 0.01, 1, and 10 mW under unsaturated conditions. For *g*-factor determination, the magnetic field was measured accurately using a nuclear magnetic resonance (NMR) detector (ES-FC5; JEOL) and a microwave counter (TR-5211A; Takeda Riken) with an experimental error of ± 0.001 mT.

Magnetic Susceptibilities Measurements. Magnetic susceptibilities of 27 mg of TPP/TEMPO IC were measured with SQUID magnetometer (MPMS-5S; QUANTUM DESIGN) in the range of 4–300 K under about 7×10^{-3} MPa helium gas flow. At first, the measurements were carried out by increasing temperature from 4.2 to 300 K, and then decreasing it. The diamagnetism of the inclusion compound was corrected using Pascal's constants.

Results and Discussion

Characterization of TPP/(TEMPO/TEMP) Inclusion Compounds. Figure 2 shows a plot of the spin concentration of TPP/TEMPO IC and TPP/(TEMPO/TEMP) IC, which is given by the integrated intensity of the resonance peak of ESR spectra (see below), against x_{TEMPO} in the preparation solution. Good correlation was shown between the spin concentration and x_{TEMPO}, suggesting that the x_{TEMPO} in TPP/(TEMPO/TEMP) IC approximately identifies that in the preparation solution. Hereafter, x_{TEMPO} is used as the molar fraction of

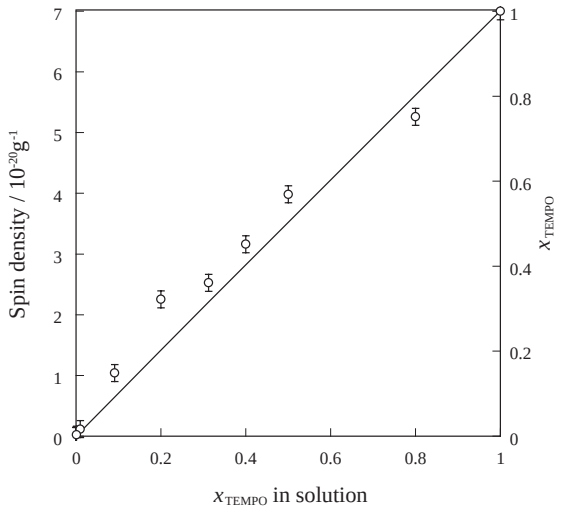

Fig. 2. Plot of the spin concentration of TPP/(TEMPO/TEMP) IC against x_{TEMPO} in the preparation solution. The solid line represents the correlation between the spin concentration and x_{TEMPO} in the preparation solution. Good correlation between these two quantities implies that the molar fraction in the preparation solution is equivalent to that in TPP/(TEMPO/TEMP) IC.

Table 1. Amount of Guest Molecule in TPP/(TEMPO/TEMP) IC Determined from Chemical Analysis

x_{TEMPO} (from spin concentration)	The amount of guest molecules in the TPP unit cell (from CA)
1.0 (TPP/TEMPO IC)	1.0
0.75	1.0
0.43	1.3
0.36	1.2
0.32	1.4
0.15	1.2
0.017	1.3
3×10^{-3}	1.3
3×10^{-5} (TPP/TEMP IC)	1.4

TEMPO in ICs.

The amount of guest molecules determined from chemical analysis of TPP/(TEMPO/TEMP) IC is listed in Table 1. The amount of guest molecules in TPP unit cell was about unity. The weight loss observed in TG also showed that a TPP unit cell accommodates one guest molecule (TEMPO and/or TEMP) for TPP/TEMPO or TPP/TEMP IC. However, in TPP/(TEMPO/TEMP) IC, the weight loss was less than one TEMPO/TEMP molecule in a TPP unit cell. In other words, the desorption of guest molecules in TPP(TEMPO/TEMP) IC does not occur smoothly in the case of mixture of TEMPO and TEMP.

Figure 3 shows the powder XRD pattern of bulk TEMPO and various TPP ICs. The reflections from bulk TEMPO (Fig. 3a) and from guest free TPP (Fig. 3b) is not visible in TPP IC as shown in Figs. 3c–3f, suggesting that no bulk TEMPO crystal remains after the preparation of TPP/TEMPO and TPP/(TEMPO/TEMP) ICs. In addition, the TPP/TEMPO IC and TPP/(TEMPO/TEMP) IC give an analog XRD pattern. Those are able to be characterized by a set of lattice parameters

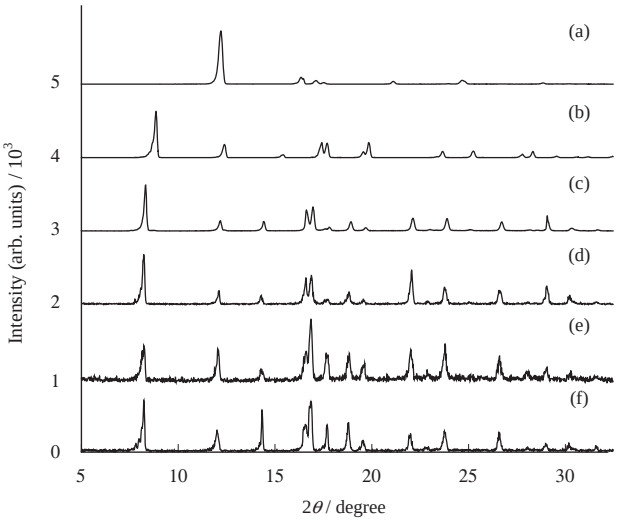

Fig. 3. Powder XRD patterns of bulk TEMPO and TPP inclusion compound: bulk TEMPO (a), guest free TPP (b), TPP/TEMPO IC (c), TPP/(TEMPO/TEMP) IC ($x_{TEMPO} = 0.36$ and 0.15) (d) and (e), and TPP/TEMP IC (f).

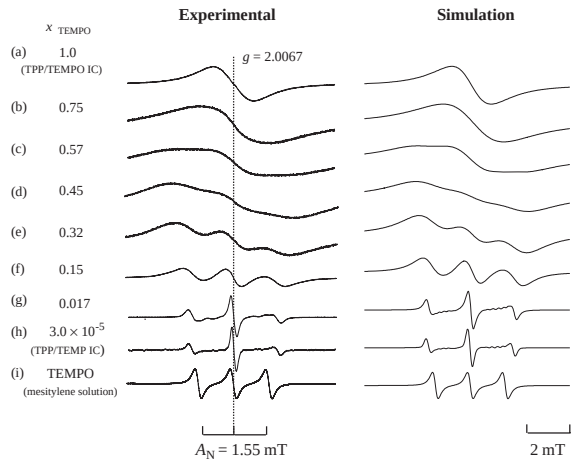

Fig. 4. Dependence of ESR spectra on x_{TEMPO} in TPP/(TEMPO/TEMP) IC: (a) $x_{TEMPO} = 1.0$ (TPP/TEMPO IC); (b) 0.75; (c) 0.57; (d) 0.45; (e) 0.32; (f) 0.15; (g) 0.017; (h) 3.0×10^{-5}; and (i) TEMPO in dilute mesitylene solution. The right column is the simulated spectra.

for monoclinic crystal with space group $P2_1/m$; $a = 1.2133$ nm, $b = 0.9830$ nm, $c = 1.2147$ nm, and $\beta = 119.95°$,[16] suggesting the existence of an isomorphic crystal of the ICs. The lattice parameters afforded a minimum nanochannel diameter of 0.58 ± 0.01 nm (in Ref. 16, the size of hydrogen atoms in benzene ring has been overestimated).

ESR Spectra in TPP/TEMPO and TPP/(TEMPO/TEMP) IC's. Figure 4 shows the powder ESR spectrum of TPP/(TEMPO/TEMP) IC at room temperature. It was found that the spectrum depended greatly on x_{TEMPO}. The ESR spectrum of TPP/TEMPO IC (Fig. 4a) exhibited an isotropic and broad resonance line; however, its character was intermediate between Gaussian and Lorentzian. The lineshape was reproduced neither by a single Gaussian nor Lorentzian, but could be reproduced by using a combination of Gaussian

(42%) and Lorentzian (58%) lineshapes. This characteristic suggests that the line broadening and lineshape did not originated from simple magnetic dipolar interaction or 3D exchange interaction, but originated from 1D exchange interaction (vide infra).

When $x_{\mathrm{TEMPO}} < 0.45$ (Figs. 4d–4h), hyperfine splitting was clearly visible, although line broadening was still present. At $x_{\mathrm{TEMPO}} = 0.017$ (Fig. 4g), the spectrum had a triplet with structure on the satellite peaks. This arrangement differs somewhat from the triplet observed in the spectrum of TEMPO in dilute mesitylene solution (Fig. 4i), in which hyperfine coupling with ^{14}N nuclei caused a triplet with equal intensity. The powder resonance line for $x_{\mathrm{TEMPO}} = 0.017$ was reproducible using a powder pattern of the triplet broadened by axial symmetric hyperfine coupling and *g*-tensors with appropriate Gaussian line broadening (see below). This lineshape was used to simulate the spectrum of samples with $x_{\mathrm{TEMPO}} < 0.45$, as shown in Figs. 4d–4h, although considerable line broadening was involved. For molar fractions of TEMPO of 0.57 and 0.75 (Figs. 4b and 4c), both spectra were reproduced by the superposition of a broad isotropic line and a powder pattern broadened by the axially symmetric *g*-tensor and hyperfine coupling tensor. This fact implied that TEMPO molecules formed two different domain structures in TPP/(TEMPO/TEMP) IC: in one domain, the molecules were arranged continuously in the TPP nanochannels and in the other domain, the TEMPO molecules were dispersed in TEMP molecules. The former afforded an ESR spectrum characterized by an isotropic and broad resonance line, whereas the latter gave a triplet that is characterized by hyperfine coupling with ^{14}N nuclei. The spectra could be reproduced when x_{TEMPO} was in the range of 0–0.45 with the hyperfine coupling tensor: $A_\perp = 1.93 \pm 0.03$ mT and $A_\parallel = 0.7 \pm 0.1$ mT, and the *g*-tensor: $g_\perp = 2.0063 \pm 0.0003$ and $g_\parallel = 2.0068 \pm 0.0005$. The orientation of the principal axes of the $\boldsymbol{A}$ and $\boldsymbol{g}$ tensors in the TPP nanochannel was unique, because a 1D nanochannel was lying along the *c*-axis and the cross section of the channel had axial symmetric with respect to the channel axis. Therefore, a parallel component in each tensor was along the channel axis and two perpendicular components were lying on the channel cross section. These tensor components afforded an isotropic value of 1.5 mT for A_{iso} $(=(2A_\perp + A_\parallel)/3)$ and 2.0065 for g_{iso} $(=(2g_\perp + g_\parallel)/3)$, which agreed well with those for TEMPO in dilute mesitylene solution within experimental error ($A_{\mathrm{N}} = 1.55$ mT and $g = 2.0069$). The anisotropy of hyperfine coupling and *g*-tensors is somewhat different from those of the TEMPO molecules in bulk crystal: $g_{xx} = 2.0103$, $g_{yy} = 2.0069$, $g_{zz} = 2.0030$ (*g*-factor only)[37,38] or in toluene glass at low-temperature ($g_{xx} = 2.0098$, $g_{yy} = 2.0062$, $g_{zz} = 2.0022$, $A_{xx} = 0.6$ mT, $A_{yy} = 0.7$ mT, $A_{zz} = 3.45$ mT) (the molecular principal axis system is depicted in Fig. 5a).[39] Furthermore, although the $\boldsymbol{A}$ and $\boldsymbol{g}$ tensors were asymmetric for an isolated TEMPO molecule, the TEMPO molecules in the TPP nanochannel had axially symmetric $\boldsymbol{A}$ and $\boldsymbol{g}$ tensors. This suggested that uni-axial molecular rotation or reorientation of TEMPO around the TPP nanochannel axis may cause the axial symmetric environment of the unpaired electron spin.

Actually, the similar behavior in $\boldsymbol{A}$ and $\boldsymbol{g}$ tensors was also observed for di-1,2-*tert*-butylnitroxide radical confined in single crystals of thiourea tubular cavity with approximately 0.7 nm diameter by Birrell et al.[40,41] The rapid molecular rotation around the channel axis causes the spin Hamiltonian to become averaged, leading to axially symmetric components in $\boldsymbol{A}$ and $\boldsymbol{g}$ tensors, as follows:

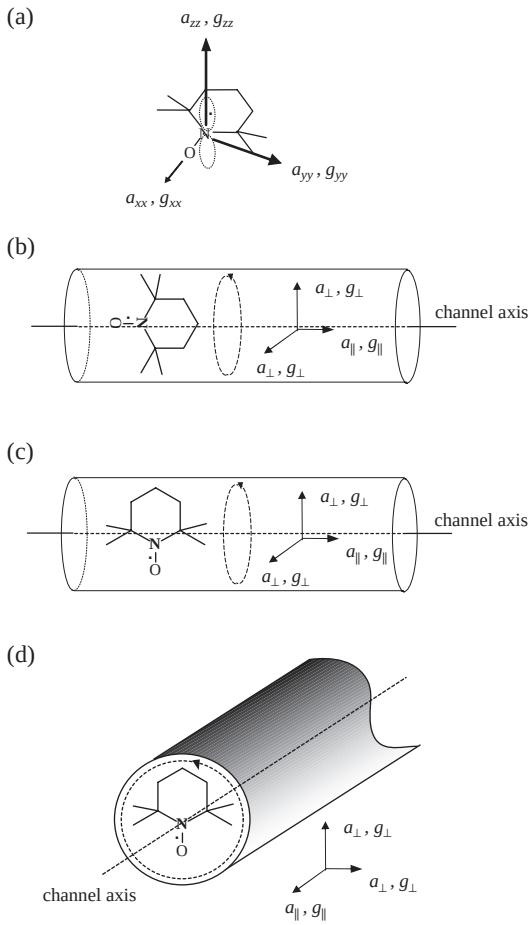

Fig. 5. The principal axes of hyperfine coupling and *g*-tensors in the TEMPO molecular frame (a), and the uni-axial rotation of TEMPO molecule around the channel axis (b)–(d). In (a), the hyperfine coupling and *g*-tensors are coaxial. The *z* axes of both tensors were laid along the direction of the N2p orbital in the SOMO. The *x* axis passes through the N–O bond; thus, the *y* axis is perpendicular to both axes. In panel (b)–(d), hyperfine coupling and *g*-tensors are axially symmetric and coaxial, and each Figures shows the axial rotation around molecular *x*, *y*, and *z* axes. The parallel component is laid along the channel axis, and the direction of perpendicular components are on the channel cross section.

$$A_\parallel = A_{ii}, \tag{1a}$$

$$g_\parallel = g_{ii}, \tag{1b}$$

$$A_\perp = \frac{1}{2}(A_{jj} + A_{kk}), \tag{1c}$$

$$g_\perp = \frac{1}{2}(g_{jj} + g_{kk}), \tag{1d}$$

where A_{ii} (g_{ii}) a is parallel component to the molecular rotation axis (channel axis), and both A_{jj} (g_{ii}) and A_{kk} (g_{kk}) are perpen-

Table 2. Principal Values of Axially Symmetric $\boldsymbol{A}$ and $\boldsymbol{g}$ Tensors of TEMPO Molecule in the TPP Nanochannels

State		$g_\perp$	$g_\parallel$	$A_\perp$/mT	$A_\parallel$/mT
Experimental		2.0063	2.0073	1.93	0.7
This study	Fig. 5b (around x axis)	2.0047	2.0099	1.97	0.75
	Fig. 5c (around y axis)	2.0061	2.0071	1.97	0.76
	Fig. 5d (around z axis)	2.0085	2.0022	0.76	3.18

dicular components to the rotation axis. In the case of di-1,2-*tert*-butylnitroxide radical in single crystals of thiourea tubular cavity, *ii*, *jj*, and *kk* correspond to *yy*, *xx*, and *zz*, respectively. These equations were applied to our system. In an isolated TEMPO molecule, the coordination systems of the principal axis of $\boldsymbol{A}$ and $\boldsymbol{g}$ tensor aligned on the TEMPO molecule as shown in Fig. 5a, which was determined by Tarasov et al. from TEMPO in glass toluene at 20–70 K.[39] When the TEMPO molecule undergoes uni-axial rotation in the 1D nanochannel, the partially averaged $\boldsymbol{A}$ and $\boldsymbol{g}$ tensors becomes axially symmetric according to Eqs. 1a–1d. We assumed three kinds of uni-axial molecular rotation for TEMPO in the TPP nanochannels along molecular axis as shown in Figs. 5b–5d. Table 2 lists the axially symmetric $\boldsymbol{A}$ and $\boldsymbol{g}$ tensor components from the experimental and the estimation from uni-axial rotation using the $\boldsymbol{A}$ and $\boldsymbol{g}$ observed at 112 K in the TPP nanochannel:[42] $g_{xx} = 2.0099 \pm 0.0002$, $g_{yy} = 2.0071 \pm 0.0002$, $g_{zz} = 2.0022 \pm 0.0002$, $a_{xx} = 0.75 \pm 0.03$ mT, $a_{yy} = 0.76 \pm 0.03$ mT, $a_{zz} = 3.18 \pm 0.03$ mT. When the y axis in tensor principal axis was parallel to the channel axis, uni-axial rotation could be used to explain the experimental results, and it was concluded that TEMPO molecule were orientated as shown in Fig. 5c.[42] Further consideration of the averaging of hyperfine coupling and g-tensors may enable us to refine the molecular orientation of TEMPO in the TPP nanochannel, and this work is now under way.

Spin Concentration Dependence of ESR Linewidth in TPP/(TEMPO/TEMP) IC. Principal axis components of the hyperfine coupling constant were independent of x_{TEMPO} from 0 to 0.45. Therefore, the TEMPO molecules were isolated by the TEMP molecule in the TPP nanochannels in these regions of x_{TEMPO}. In this case, the ESR line width was thought to result from dipolar interaction. Figure 6 shows dependence of the line broadening of the ESR spectrum in TPP/(TEMPO/TEMP) IC on the square root of x_{TEMPO}. The ESR signal was observed even in TPP/TEMP IC because of a trace amount of TEMPO resulting from the oxidization of TEMP by heating.[43–45] Although the resonance line of this specimen was characterized mainly by hyperfine coupling with ^{14}N nuclei, line broadening of 0.21 mT was caused by dipolar interactions in the TPP framework (solid line (A) in Fig. 6). This 0.21 mT broadening should incorporate a contribution from dipolar broadening because of the ^{1}H spins in the TPP framework in all samples. The resonance line was broadened when x_{TEMPO} increased. Maximum broadening of 2.2 mT was observed on the resonance line for the isolated TEMPO molecule, when x_{TEMPO} was in the range of 0.5–0.6 ($\sqrt{x_{\mathrm{TEMPO}}} \approx 0.7$–$0.8$). After maximum broadening, the peak-to-peak linewidth decreased again with increasing x_{TEMPO} toward 1.8 mT. The increase in the linewidth when $\sqrt{x_{\mathrm{TEMPO}}} < 0.7$ can be explained by

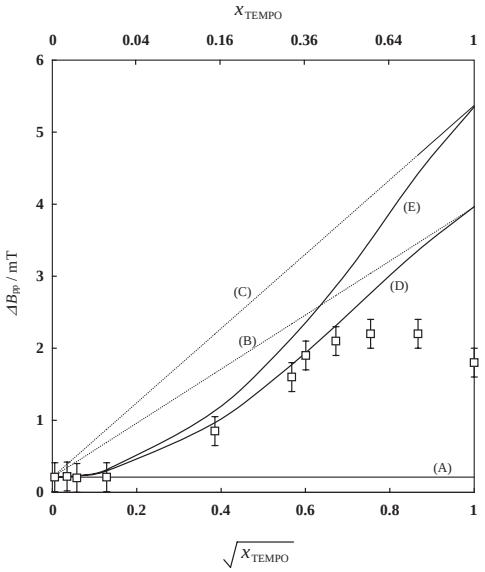

Fig. 6. Dependence of the linewidth of the ESR spectra of TPP/(TEMPO/TEMP) IC on the molar fraction of TEMPO. The horizontal axes are taken by the square root of x_{TEMPO} in the preparation solution to all the guest compounds. Experimental linewidth is depicted as a solid square. Solid horizontal line (A) shows dipolar broadening by ^{1}H in the TPP lattice. Dashed lines (B) and (C) respectively show the expected line broadening by the average magnetic dipolar interaction from the intrachain, and intrachain and interchain. Solid curves (D) and (E) respectively show the line broadening evaluated from the intrachain, and the intrachain and inter-chain magnetic dipolar interaction using Eqs. 4–7.

the dipolar interaction between electron spins on TEMPO molecules.

In TPP/TEMPO IC and TPP/(TEMPO/TEMP) IC, the electron spin interacted with spins in the same channel and in adjacent channels. The former is intrachain interaction, and the latter is interchain interaction in this paper. The average line broadening from these magnetic dipolar interactions can be estimated from the second moment of the resonance line using spin concentration and the Van Vleck formula;[46]

$$M_2 = \Delta\omega^2 = \frac{3}{5} x_{\mathrm{TEMPO}} (g\beta)^4 \left(\frac{1}{\hbar}\right)^2 S(S+1) \sum_k \left(\frac{1}{r_{jk}}\right)^6, \quad (2)$$

where g denotes the g-factor of electron, β is the Bohr magneton, and r_{jk} is the distance between two spins. The position of the electron spin was assumed to be in the center of gravity of TEMPO molecule in the TPP nanochannel, because of averaging by the rapid axial rotation of TEMPO molecule around the

channel axis. The averaged interspin distance was estimated to be 0.98 nm for intrachain TEMPO's and 1.2 nm for interchain TEMPO's, if the TPP unit cell contains one TEMPO molecule in TPP/TEMPO IC and if all TEMPO molecules (that is, all electron spins) exist in the same lattice point. The second moment M_2 is proportional to the spin concentration. Equations 3a and 3b show the expected line broadening for the Gaussian absorption line: the former is full width of half maximum (FWHM), and the latter is peak-to-peak linewidth.

$$\Delta B_{1/2} = 2.36\sqrt{M_2}, \tag{3a}$$

$$\Delta B_{\mathrm{pp}} = 2\sqrt{M_2}. \tag{3b}$$

That is, the relation $\Delta B_{1/2} = 1.18\Delta B_{\mathrm{pp}}$ was derived. In this paper, the term of linewidth expresses the peak-to-peak linewidth. According to Eqs. 2 and 3b, ΔB_{pp} varies linearly with $\sqrt{x_{\mathrm{TEMPO}}}$. Expected line broadening from Eqs. 2 and 3b, which include the intrachain and interchain contributions, increased linearly as a function of $(x_{\mathrm{TEMPO}})^{1/2}$. Estimated contributions from the intrachain interaction and from the sum of interchain and intrachain interaction are depicted respectively as dashed lines (B) and (C) in Fig. 6. Apparently, average line broadening based on x_{TEMPO} cannot be used to interpret the experimental results.

In fact, the linewidth was influenced effectively by the nearest neighbors of a given TEMPO molecule. For the intrachain interaction, there are three kinds of molecular configuration of the adjacent sites of a given TEMPO molecule: (a) TEMP–TEMPO–TEMP, (b) TEMPO–TEMPO–TEMP, and (c) TEMPO–TEMPO–TEMPO. If the number of TEMPO molecules occupying the adjacent sites of a TEMPO molecule is denoted as n, then $n = 0$ for (a), $n = 1$ for (b), and $n = 2$ for (c). If the TEMPO molecules distribute statistically in the molecular chain of the mixture of TEMPO and TEMP in relation to x_{TEMPO}, the probability of finding each configuration can be represented as a function of x_{TEMPO}. In this case, the second moment, $M_{2(\mathrm{intra})}$, is given as the weighted average of the inherent M_2 among these configurations as

$$M_{2(\mathrm{intra})} = \sum_{n=0}^{2} {p_n}^{\mathrm{intra}} {M_2}^{\mathrm{intra}}(n). \tag{4}$$

In that equation, $M_2(n)$ is the inherent second moment for each configuration, and ${p_n}^{\mathrm{intra}}$ is represented by the binomial distribution shown in Eq. 5.

$$p_n^{\mathrm{intra}} = \binom{2}{n}(1 - x_{\mathrm{TEMPO}})^{2-n} {x_{\mathrm{TEMPO}}}^n. \tag{5}$$

This treatment is also valid for interchain interaction, in which the six nearest neighboring sites are taken into account. In this case, seven possible configurations are available. Similarly, the second moment, $M_{2(\mathrm{inter})}$, which is attributable to interchain interaction, is given as the following:

$$M_{2(\mathrm{inter})} = \sum_{n=0}^{6} p_n^{\mathrm{inter}} M_2^{\mathrm{inter}}(n). \tag{6}$$

In that equation, ${p_n}^{\mathrm{inter}}$ represents the value shown in Eq. 7.

$$p_n^{\mathrm{inter}} = \binom{6}{0}(1 - x_{\mathrm{TEMPO}})^{6-n} {x_{\mathrm{TEMPO}}}^n. \tag{7}$$

In addition, ${M_2}^{\mathrm{intra}}(n)$ and ${M_2}^{\mathrm{inter}}(n)$ are evaluated using the Van Vleck formula.[46] Using Eqs. 4–7, line broadening based on the intrachain interaction and/or the sum of the intrachain and interchain interactions could be estimated as drawn by solid lines (D) and (E), respectively, in Fig. 6. At a low concentration of TEMPO, the configuration (a) was the dominant local structure of TEMPO in the TPP nanochannels, implying that the linewidth is approximately independent of x_{TEMPO}. When the TEMPO concentration was higher, the populations of configurations (b) and (c) increased, and an increase in the linewidth occured. Up to $\sqrt{x_{\mathrm{TEMPO}}} \approx 0.6$, solid line (D) in Fig. 6, the broadening from the intrachain dipolar interaction agreed better with the experimental linewidth. The interspin distance in the interchain TEMPO was about 20% larger than that in the intrachain spins. In addition, the effect of interchain dipolar interaction was statistically weak in the low x_{TEMPO} range according to Eqs. 6 and 7. These implied that the dipolar interaction from the intrachain spins dominantly attributes to the linewidth.

Exchange Narrowing of ESR Resonance Line in TPP/(TEMPO/TEMP) IC. When $\sqrt{x_{\mathrm{TEMPO}}} > 0.6$, the intrachain and interchain dipolar interactions are expected to increase the linewidth of the ESR spectra. However, the linewidth of TPP/(TEMPO/TEMP) IC in this x_{TEMPO} range decreased with an increase in x_{TEMPO}; especially in TPP/TEMPO IC, the experimental linewidth was 3.5 mT narrower than that predicted by intrachain and interchain dipolar interaction. This suggests that an additional narrowing mechanism acts on the ESR spectrum. Generally, two narrowing mechanisms can influence the ESR lineshape: motional narrowing and/or exchange narrowing. However, since we assumed the averaging of dipolar interaction through uni-axial rotation of the TEMPO molecules in the TPP nanochannel, the effect of motion on the linewidth was already included in the analysis. In addition, complete motional narrowing commonly gives a Lorentzian lineshape, whereas exchange narrowing gives a characteristic lineshape depending on the dimensionality of exchange interaction: Lorentzian for 3D exchange interaction, and a mixture of Lorentzian and Gaussian for 1D or 2D. The lineshape of TPP/TEMPO IC at room temperature was not Lorentzian, but intermediate between Lorentzian and Gaussian. A lineshape including 42% Gaussian and 58% Lorentzian lines could be used to reproduce the experimental lineshape at room temperature, suggesting that exchange narrowing was active in this x_{TEMPO} region. Thus, we examined temperature dependence of ESR spectra in the temperature range from 12 to 383 K in order to clarify the narrowing mechanism of TPP/TEMPO IC.

Figure 7 shows temperature dependence of ΔB_{pp} of TPP/TEMPO IC. The dashed horizontal line shows estimation of the line broadening from only the intrachain dipolar interaction ($\Delta B_{\mathrm{pp}} = 4.0$ mT), whereas solid horizontal line shows estimation of the line broadening from both intrachain and interchain dipolar interactions ($\Delta B_{\mathrm{pp}} = 5.3$ mT) based on the model described above. When $T < 100$ K, the linewidth was almost constant ($\Delta B_{\mathrm{pp}} = 4.8$ mT) and was close to sum of the dipolar broadening from both intrachain and interchain dipolar interactions. In this temperature range, molecular motion is commonly expected to be frozen, but the experimental linewidth was narrower than the estimation under the uni-axial rotation

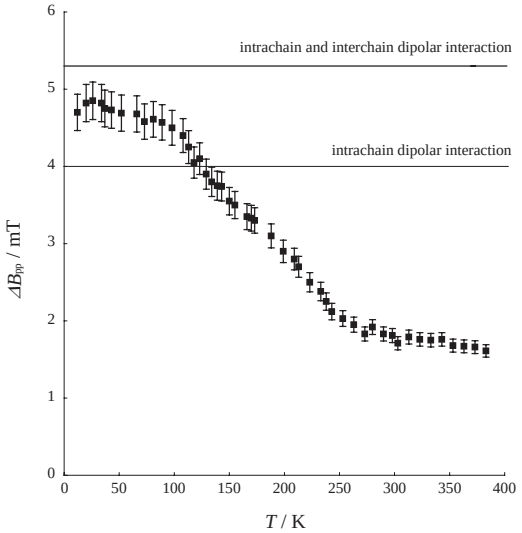

Fig. 7. Temperature dependence of peak-to-peak linewidth of TPP/TEMPO IC in 12–383 K.

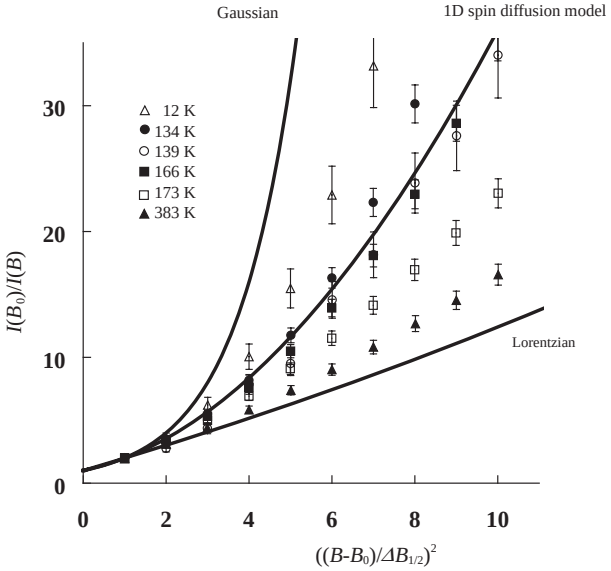

Fig. 8. Temperature dependence of lineshape of TPP/TEMPO IC in 12–383 K by Dietz's plot.[46]

condition. In other words, exchange narrowing appeared to take place even after freezing the molecular motion. When $T > 100$ K, the linewidth decreased as temperature increased, and when $T > 270$ K, the linewidth became almost constant again ($\Delta B_{pp} = 1.8$ mT). The TPP nanochannels are very crowded because it fully accommodates TEMPO and/or TEMP molecules, resulting in a smaller contribution from the diffusion of TEMPO molecule. Since the effect of motional narrowing was already considered in the estimation of dipolar interaction averaged by the axial rotation of TEMPO molecule in the TPP nanochannel (see above), the narrowing in this temperature range was expected to originate from only exchange interaction, especially from 1D exchange interaction, because of the 1D molecular arrangement of TEMPO molecules in the TPP nanochannel. Anisotropic dimensionality of the exchange interaction caused the characteristic lineshape of the ESR peak, which was intermediate between Lorentzian and Gaussian for 1D exchange interaction.

Dimensionality of Exchange Interaction in TPP/TEMPO IC. In order to examine the dimensionality of exchange interaction of TPP/TEMPO IC, we investigated the temperature dependence of the lineshape of the resonance line by using a Dietz's plot,[47] in which $I(B_0)/I(B)$ is plotted against $[(B - B_0)/\Delta B_{1/2}]$ (see Fig. 8). The resonance line of the ESR spectrum was obtained by the Fourier transformation of the relaxation function of transverse magnetization, $\phi(t)$: (1) in the absence of an exchange interaction between two spins, $\phi(t)$ is described by a Gaussian function, resulting in a Gaussian resonance line, (2) in a three-dimensionally interacting spin system by exchange or motional averaging, the spin correlation function rapidly decays to zero, leading to the exponential function for $\phi(t)$ and a Lorentzian resonance line, (3) in the extreme narrowing regime, where the timescale is much longer than the correlation time of the fluctuation of spins ($\tau_e \ll t$), $\phi(t)$ is determined by the long time tail of the correlation function of the local field ($\Psi(\tau)$) and the microscopic behavior of the spin system is described by the so-called "spin-diffusion" process.[47–51] As the dimensionality of the spin interaction lowers, the decay in the spin correlation function is slower and the long time behavior characterizes the lineshape of the resonance peak. For a 1D-spin system, $\phi(t) \propto \exp[-(\Gamma t)^{3/2}]$, and this relaxation function gives an intermediate lineshape between Gaussian and Lorentzian.

Figure 8 shows Dietz's plot of TPP/TEMPO IC at some appropriate temperature. In the temperature range from 12 to 139 K, the lineshape was between a pure Gaussian lineshape and the lineshape from the 1D spin diffusion model, suggesting that 1D spin diffusion mechanism was still active even at quite low temperatures, at which molecular rotation of TEMPO in the TPP nanochannel is frozen. In the range of 139–166 K, the lineshape of TPP/TEMPO IC is good agreement with pseudo-1D-spin diffusion model, and therefore, an exchange narrowing mechanism can be used to describe the narrowing shown in Fig. 8. At $T > 166$ K, the resonance peak became more Lorentzian as the temperature increased, but it did not become pure Lorentzian even at 383 K. The increase in the contribution of Lorentzian character suggests that anisotropic exchange interaction effectively comes from interchain spins. The interchain interaction cuts off $\Psi(\tau)$ after a characteristic time. The lineshape at 383 K can be used to estimate roughly the ratio of intrachain exchange interaction (J_{intra}) to interchain exchange interaction (J_{inter}) to be $J_{inter}/J_{intra} \approx 10^{-2}$–$10^{-3}$.[48,50] This finding implies that the exchange interaction in TPP/TEMPO IC seems to be affected by uni-axial rotation of TEMPO molecule in the TPP nanochannel. Thus, in this system, uni-axial rotation of TEMPO contributes to the exchange narrowing of the ESR lineshape. The motional averaging of the molecular orientation of TEMPO in the nanochannel gave rise to a homogeneous environment of TEMPO local structure, probably leading to homogeneous overlap of the wave functions for unpaired electrons between adjacent molecules. This situation causes a large exchange integral, resulting in an increase in exchange narrowing. Thus, TPP/TEMPO IC is quite a remarkable material, in which the dimensionality of exchange interaction changes from 1D to 3D with an increase in the tem-

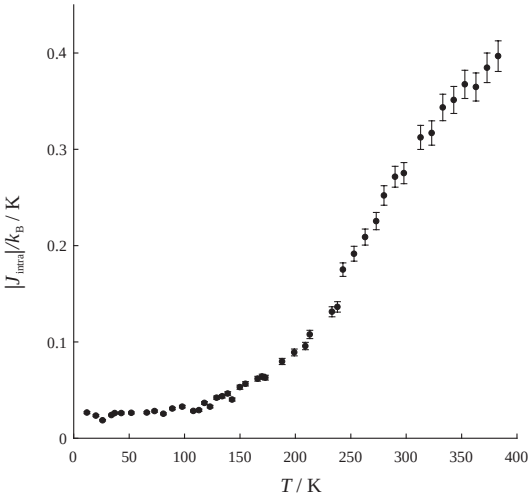

Fig. 9. Temperature dependence of $|J_{intra}|/k_B$ of TPP/TEMPO IC estimated by Eq. 8.

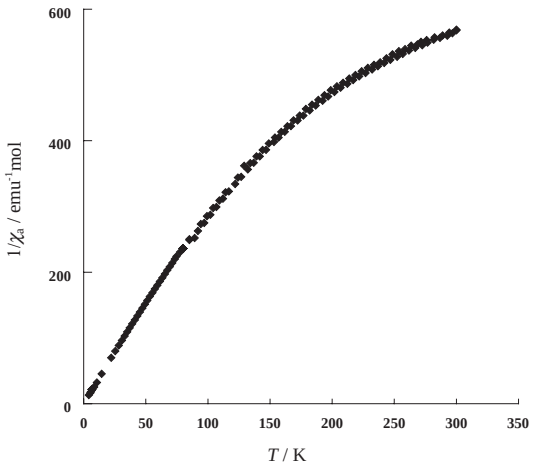

Fig. 10. T versus $1/\chi_a$ after diamagnetic correction in 4–300 K.[59]

perature, in contrast to the known 1D magnetic material.[51,52]

Estimation of the Magnitude of the Exchange Interaction and Macroscopic Magnetic Properties of the TPP/TEMPO Inclusion Compound. In the 1D spin chain, the FWHM ($\Delta B_{1/2}$) of the resonance line in the ESR spectrum is represented by the following equation:

$$\Delta B_{1/2} = 3.488 \frac{{M_2}^{2/3}}{(|J_{intra}|/\hbar)^{1/3}}, \quad (8)$$

where M_2 is the second moment of the resonance line of the ESR spectrum in the rigid lattice,[46] and $|J_{intra}|$ is the magnitude of the exchange interaction in the intrachain contribution. Although, in TPP/TEMPO IC, pure 1D spin diffusion was observed only in 139–166 K, this system had 1D character of exchange interaction over all temperature ranges. Therefore, Equation 8 could be used over all temperature ranges to estimate the magnitude of the exchange interaction. Figure 9 shows temperature dependence of $|J_{intra}|/k_B$ of TPP/TEMPO IC. When $T < 120$ K, $|J_{intra}|/k_B$ was between 0.02 and 0.03 K, and seems to be independent of temperature. When $T > 120$ K, $|J_{intra}|/k_B$ increased monotonically with an increase in the temperature. In the temperature range from 139 to 166 K (1D spin diffusion range), $|J_{intra}|/k_B$ was estimated to be about 0.05 K. Thus, although $|J_{intra}|/k_B$ of TPP/TEMPO IC was much smaller than a metal magnet ($|J_{intra}|/k_B > 10$ K), a finite $|J_{intra}|/k_B$ was observed. Therefore, TPP/TEMPO IC was determined to be a magnetic IC, in which 1D spin chain is constructed by the spin localized in only the 2p orbital, and it is quite a remarkable IC because the magnitude and/or dimensionality of exchange interaction changes depending on temperature, that is, molecular motion of guest molecule contributes to the exchange interaction. The maximum magnitude of $|J_{intra}|/k_B$ was 0.4 K at 383 K. This $|J_{intra}|/k_B$ is comparable to those in some bulk organic crystals. Antiferromagnetic exchange interaction ($J/k_B \approx -1.8$ K[53]) has been observed for bulk TEMPO crystals and a solid solution of DPPH in polystyrene, which is a type of molecular assembly similar to our system ($J/k_B \approx 1$ K).[54,55] In addition, the $|J_{intra}|/k_B$ of TPP/TEMPO IC is also similar to that of phenyl–CH≡N–TEMPO crystal ($J/k_B \approx 0.2$ K) reported by Kawakami and co-workers.[56] In phenyl–CH≡N–TEMPO crystal, it has been proposed that the exchange interaction takes place through space of 0.5 nm, which is the interspin distance. In contrast, in TPP/TEMPO IC, the exchange interaction takes place through a space of 1.0 nm along a 1D spin chain, which is twice of the interspin distance in phenyl–CH≡N–TEMPO crystal. This enlarged interspin distance gave a smaller value of $|J_{intra}|/k_B$ for TPP/TEMPO IC in the temperature range of the pure 1D spin diffusion process. However, above room temperature, $|J_{intra}|/k_B$ of TPP/TEMPO IC was of the same order of magnitude as phenyl–CH≡N–TEMPO. Therefore, the mechanism for 1D spin exchange assisted by molecular motion is more complex than the through-space exchange interaction.

Figure 10 shows temperature dependence of the inverse of molar magnetic susceptibility (χ_a) of TPP/TEMPO IC. Up to 80 K, the reciprocal susceptibility increased linearly as the temperature increased. In this temperature range, dipolar interaction was dominated by interspin interaction, and magnetism of TPP/TEMPO IC was approximately paramagnetic. On the basis of the ESR linewidth, the magnitude of exchange interaction was evaluated to be 0.02–0.03 K. These values are too small to affect the temperature dependence of χ_a. Therefore, the magnetic susceptibility seems to obey Curie's law below about 100 K. However, when $T > 100$ K, the temperature dependence of $1/\chi_a$ was small. That is, the slope of temperature dependence of $1/\chi_a$ was smaller than that in the temperature range below 80 K as increase in temperature. Therefore, intrachain exchange interaction was expected to be antiferromagnetic, that is, $J_{intra} < 0$ in $T > 100$ K. Since $|J_{intra}|$ depends on temperature, conventional Curie–Weiss law, or 1D ferro/antiferromagnetic spin chain model[57,58] cannot be applied. This trend was also reproduced in other samples. This temperature dependence of magnetic susceptibilities is probably related to the frequency of molecular reorientation of TEMPO in the TPP nanochannel. The relationship between the magnetic susceptibilities of TPP/TEMPO IC and the molecular rotation correlation time of TEMPO in the TPP nanochannel should help to understand molecular magnets constructed in a template such as porous materials. The molecular rotation correla-

tion time is estimated by measuring the temperature dependence of the ESR lineshape in TPP/(TEMPO/TEMP) IC ($n = 0.017$). Assuming the analogue molecular motion of TEMP to TEMPO in the TPP nanochannel, it may be possible to determine the correlation time of TEMP in the TPP nanochannel by using the lineshape analysis of ^{2}H NMR spectrum of TPP/TEMP-d_1. Further analysis for the temperature dependence of the magnetic susceptibilities is now under way.

Conclusion

We conducted powder ESR measurements on novel ICs of TPP with a stable organic radical, TEMPO, in order to investigate spin–spin interaction and the magnetic properties. The spin concentration dependence of the spin–spin interaction was examined by dilution of TEMPO with diamagnetic TEMP.

Results showed that the ESR lineshape of each spectrum depended on x_{TEMPO}. When $x_{\mathrm{TEMPO}} < 0.45$, the ESR spectrum was defined by axially symmetric hyperfine coupling and g-tensors, suggesting that the TEMPO molecule is isolated in the TEMP matrix and undergoes uni-axial rotation around a channel axis. For $x_{\mathrm{TEMPO}} < 0.7$, the resonance line of the ESR spectrum was broadened mainly due to intrachain magnetic dipolar interaction, whereas for $x_{\mathrm{TEMPO}} > 0.7$, the exchange narrowing was remarkable. Lineshape analysis supported 1D exchange narrowing for TPP/TEMPO IC.

Furthermore, temperature dependence of the lineshape clearly showed that exchange narrowing increased with temperature. This finding suggested that the exchange interaction was affected by uni-axial rotation of TEMPO molecules. In the temperature range from 12 to 383 K, 1D spin diffusion contributed to the exchange narrowing. Especially, between 139 and 166 K, pure 1D spin diffusion occured. On the basis of the 1D spin diffusion model, we estimated the magnitude of the exchange interaction between the intrachain spins: $|J_{\mathrm{intra}}|/k_{\mathrm{B}} \approx 0.05$ K in the temperature range of pure 1D spin diffusion and maximum $|J_{\mathrm{intra}}|/k_{\mathrm{B}} \approx 0.4$ K at 383 K. From the temperature dependence of χ_{a}, the spin–spin interaction was determined to be antiferromagnetic, that is, the negative sign for $|J_{\mathrm{intra}}|/k_{\mathrm{B}}$.

This work was partially supported by a Grant-in-Aid for Scientific Research (No. 16550013) from the Japanese Ministry of Education, Culture, Sports, Science and Technology. We thank Professor W. Mori at Kanagawa University for the help of the measurement of magnetic susceptibility.

References

1 B. Ye, M. Trudeau, D. M. Antonelli, *Adv. Mater.* **2001**, *13*, 29.

2 B. Ye, M. L. Trudeau, D. M. Antonelli, *Adv. Mater.* **2001**, *13*, 561.

3 F. Marlow, M. Wübbenhorst, J. Caro, *J. Phys. Chem.* **1994**, *98*, 12315.

4 G. J. Halder, C. J. Kepert, B. Moubaraki, K. S. Murray, J. D. Cashion, *Science* **2002**, *298*, 1762.

5 R. Kitaura, S. Kitagawa, Y. Kubota, T. C. Kobayashi, K. Kindo, Y. Mita, A. Matsuo, M. Kobayashi, H.-C. Chang, T. C. Ozawa, M. Suzuki, M. Sakata, M. Takata, *Science* **2002**, *298*, 2358.

6 M. N. Leunberger, D. Loss, *Nature* **2001**, *410*, 789.

7 R. Clérac, H. Miyasaka, M. Yamashita, C. Coulon, *J. Am. Chem. Soc.* **2002**, *124*, 12837.

8 A. Caneschi, D. Gatteschi, N. Lalioti, C. Sangregorio, R. Sessoli, G. Venturi, A. Vindigni, A. Rettori, M. G. Pini, M. A. Novak, *Angew. Chem., Int. Ed.* **2001**, *40*, 1760.

9 R. Lescouëzec, J. Vaissermann, C. Ruiz-Pérez, F. Lloret, R. Carrasco, M. Julve, M. Verdaguer, Y. Dromzee, D. Gatteschi, W. Wernsdorfer, *Angew. Chem., Int. Ed.* **2003**, *42*, 1483.

10 K. Miyajima, A. Nakajima, S. Yabushita, M. B. Knickelbein, K. Kaya, *J. Am. Chem. Soc.* **2004**, *126*, 13202.

11 H. Miyasaka, T. Nezu, K. Sugimoto, K. Sugiura, M. Yamashita, R. Clérac, *Inorg. Chem.* **2004**, *43*, 5486.

12 H. Miyasaka, R. Clérac, K. Mizushima, K. Sugiura, M. Yamashita, W. Wernsdorfer, C. Coulon, *Inorg. Chem.* **2003**, *42*, 8203.

13 R. J. Glauber, *J. Math. Phys.* **1963**, *4*, 294.

14 D. Gatteschi, R. Sessoli, *J. Magn. Magn. Mater.* **2004**, *272–276*, 1030.

15 C. Coulon, R. Clérac, L. Lecren, W. Wernsdorfer, H. Miyasaka, *Phys. Rev. B* **2004**, *69*, 132408.

16 H. Kobayashi, T. Ueda, K. Miyakubo, J. Toyoda, T. Eguchi, A. Tani, *J. Mater. Chem.* **2005**, *15*, 872.

17 P. Sozzani, S. Bracco, A. Comotti, L. Ferretti, R. Simonutti, *Angew. Chem., Int. Ed.* **2005**, *44*, 1816.

18 H. R. Allcock, *J. Am. Chem. Soc.* **1964**, *86*, 2591.

19 H. R. Allcock, *Inclusion Compounds*, ed. by J. L. Atwood, J. E. D. Davies, D. D. MacNicol, Academic Press Inc., London, **1984**, Vol. 1, pp. 351–374.

20 H. R. Allcock, *Chem. Rev.* **1972**, *72*, 315.

21 H. R. Allcock, L. A. Siegel, *J. Am. Chem. Soc.* **1964**, *86*, 5140.

22 L. A. Siegel, J. H. van den Hende, *J. Chem. Soc. A* **1967**, 817.

23 H. R. Allcock, R. W. Allen, E. C. Bissell, L. A. Smeltz, M. Teeter, *J. Am. Chem. Soc.* **1976**, *98*, 5120.

24 H. R. Allcock, M. L. Levin, R. R. Whittle, *Inorg. Chem.* **1986**, *25*, 41.

25 T. Hertzsch, F. Budde, E. Weber, J. Hulliger, *Angew. Chem., Int. Ed.* **2002**, *41*, 2281.

26 T. Hertzsch, S. Kluge, E. Weber, F. Budde, J. Hulliger, *Adv. Mater.* **2001**, *13*, 1864.

27 H. I. Süss, T. Wuest, A. Sieber, R. Althaus, F. Budde, H.-P. Lüthi, G. D. McManus, J. Rawson, J. Hulliger, *CrystEngComm* **2002**, *4*, 432.

28 G. Wolmershäuser, R. Johann, *Angew. Chem., Int. Ed. Engl.* **1989**, *28*, 920.

29 W. Fujita, K. Awaga, *Science* **1999**, *286*, 261.

30 G. D. McManus, J. M. Rawson, N. Feeder, J. van Duijn, E. J. L. McInnes, J. J. Novoa, R. Burriel, F. Palacio, P. Oliete, *J. Mater. Chem.* **2001**, *11*, 1992.

31 D. Bordeaux, J. Bornarel, A. Capiomont, J. Lajzerowicz-Bonneteau, J. Lajzerowicz, J. F. Legrand, *Phys. Rev. Lett.* **1973**, *31*, 314.

32 A. Capiomont, J. Lajzerowicz-Bonneteau, *Acta Crystallogr., Sect. B* **1974**, *30*, 2160.

33 M.-S. Jang, T. Nakamura, M. Takashige, S. Kojima, *Jpn. J. Appl. Phys.* **1980**, *19*, 1413.

34 J. F. W. Keana, *Chem. Rev.* **1978**, *78*, 37.

35 H. Kobayashi, T. Ueda, K. Miyakubo, T. Eguchi, *Z. Naturforsch., A: Phys. Sci.* **2003**, *58*, 727.

36 M. Tinkham, M. W. P. Strandberg, *Phys. Rev.* **1955**, *97*, 937.
37 D. Bordeaux, J. Lajzerowicz-Bonneteau, *Org. Magn. Reson.* **1973**, *5*, 47.
38 J. S. Hwang, R. P. Mason, L.-P. Hwang, J. H. Freed, *J. Phys. Chem.* **1975**, *79*, 489.
39 V. F. Tarasov, I. A. Shkrob, A. D. Trifunac, *J. Phys. Chem. A* **2002**, *106*, 4838.
40 G. B. Birrell, S. P. Van, O. H. Griffith, *J. Am. Chem. Soc.* **1973**, *95*, 2451.
41 L. J. Libertini, O. H. Griffith, *J. Chem. Phys.* **1970**, *53*, 1359.
42 H. Kobayashi, T. Ueda, K. Miyakubo, T. Eguchi, A. Tani, to be submitted.
43 L. Guo, K. Chen, H. Tian, *Chem. Eng. Technol.* **2001**, *24*, 181.
44 H. Tian, K. C. Chen, L. Guo, *J. East China Univ. Sci. Technol.* **1999**, CN 1235946A.
45 V. D. Sen, V. A. Golubev, N. N. Efremora, *Izv. Akad. Nauk SSSR, Ser. Khim.* **1982**, 61.
46 A. Abragam, *Principles of Nuclear Magnetism*, Oxford, New York, **1961**, p. 112.
47 R. E. Dietz, F. R. Merritt, R. Dingle, D. Hone, B. G. Silbernagel, P. M. Richards, *Phys. Rev. Lett.* **1971**, *26*, 1186.
48 M. J. Hennessy, C. D. McElwee, P. M. Richards, *Phys. Rev. B* **1973**, *7*, 930.
49 J.-P. Boucher, M. A. Bakheit, M. Nechtshein, M. Villa, G. Bonera, F. Borsa, *Phys. Rev. B* **1976**, *13*, 4098.
50 T. T. P. Cheung, Z. G. Soos, R. E. Dietz, F. R. Merritt, *Phys. Rev. B* **1978**, *17*, 1266.
51 A. Caneschi, D. Gatteschi, R. Sessoli, C. I. Cabello, P. Rey, A. L. Barra, L. C. Brunel, *Inorg. Chem.* **1991**, *30*, 1882.
52 A. Caneschi, D. Gatteschi, P. Rey, R. Sessoli, *Inorg. Chem.* **1988**, *27*, 1756.
53 J. Yamauchi, *Bull. Chem. Soc. Jpn.* **1971**, *44*, 2301.
54 J. P. Goldsborough, M. Mandel, G. E. Pake, *Phys. Rev. Lett.* **1960**, *4*, 13.
55 G. E. Pake, T. L. Estle, *The Physical Principles of Electron Paramagnetic Resonance*, 2nd ed., W. A. Benjamin, Inc., Massachusetts, **1973**, p. 171, and references therein.
56 T. Kawakami, A. Oda, S. Takada, W. Mori, T. Ishida, M. Yasui, F. Iwasaki, T. Nogami, K. Yamaguchi, *Mol. Cryst. Liq. Cryst.* **1997**, *306*, 141.
57 G. A. Baker, Jr., G. S. Rushbrooke, H. E. Gilbert, *Phys. Rev.* **1964**, *135*, A1272.
58 J. C. Bonner, M. E. Fisher, *Phys. Rev.* **1964**, *135*, A640.
59 χ_a is given by emu mol^{-1} unit. Multiplying $4\pi \times 10^{-6}$ gives the corresponding value in SI unit.